Effects of vacancy defects on graphene nanoribbon field effect transistor

Sheng Chang[1], Yajun Zhang[1], Qijun Huang[1], Hao Wang[2], Gaofeng Wang[2]

[1]*School of Physics and Technology, Wuhan University, Wuhan 430072, People's Republic of China*
[2]*School of Electronics and Information, Hangzhou Dianzi University, Hangzhou 310018, People's Republic of China*
E-mail: gaofeng@whu.edu.cn

Published in Micro & Nano Letters; Received on 25th July 2013; Revised on 19th October 2013; Accepted on 22nd October 2013

The graphene nanoribbon (GNR) field effect transistor is one of the most competitive candidates for beyond-CMOS nanoelectronics because of the special electric characteristics of graphene. During graphene preparation, vacancy defects are inevitably introduced and affect transistor performances. In this Letter, four typical vacancy defects in GNR (i.e. single vacancy, divacancy, Stone-Wales and 555 777 defects) are examined. By quantum-mechanics-based simulation, the effects of these four defects on the energy band of the GNR are analysed. Moreover, their effects on the performances of the GNR field effect transistor, such as transmission coefficient and transfer characteristics, are studied and compared for various defect locations in the channel.

1. Introduction: Graphene has attracted a great deal of attention because of its special physical and electric characteristics since it was reported in 2004 [1]. Graphene-based semiconductor devices have become a hot research topic. A number of graphene devices, such as back-gate, top-gate and double-gates structures, were fabricated [2–4]. Since graphene is a zero bandgap material, it could be tailored as a narrow ribbon in nanoscale for opening bandgap [5]. As a result, the tailored graphene nanoribbon (GNR) can achieve a ratio of I_{on}/I_{off} as high as 10^7 [6]. Based on this phenomenon, the GNR field effect transistor (GNRFET) has become a focus of recent studies [7–9], and is considered as a promising candidate for the next generation logic circuits.

In the preparation of GNR, it is hard to avoid defects. Various defects, such as vacancy defects [10–12], impurity defects [13, 14] and adsorption defects [15, 16], could be introduced. Inevitably, these defects can influence the characteristics of the GNR, such as energy band structure, carrier mobility, conductivity and so on. The vacancy defects, which are a very basic type of defect, are discussed here.

So far, studies about the vacancy defects mostly focus on their influences on the material properties of GNR, whereas effects of the vacancy defects on device characteristics are rarely investigated. For example, defect-caused scattering in epitaxial graphene was discussed in [17], while how the density of vacancies affects the density of state was studied in [18]. However, both studies did not focus on GNR. Electronic transport at the vacancy defected GNR was studied in [19], but no specific defect type was given. The effect of the single lattice defect on the GNR's conductance was studied in [20, 21], while the effect of the single lattice defect on the GNR's potential distribution was investigated in [22]. It was illustrated in [23, 24] that the locations of two single vacancies (SVs) have considerable effect on the GNR's electronic transport properties. However, no other types of vacancy defects were considered in these works. In [25], the effect of the Stone-Wales (SW) defect on spin-dependent electronic transport in zigzag GNR (ZGNR) was analysed, without further examining the related device characteristics. The influence of the vacancy defects was mentioned in [26] for performance comparison of GNR Schottky barrier gate field effect transistors (FETs) and metal-oxide-semiconductor FETs, but there is a lack of a comprehensive study.

In this Letter, the effects of the vacancy defects on the GNRFET are studied comprehensively. All four types of the most common vacancy defects, that is, the SV defect, the divacancy (DV) defect, the SW defect and the 555 777 defect, are discussed and compared. By quantum-mechanics-based simulation, their effects on the GNRFET (a three-terminal device) are analysed from the aspect of device characteristics. This is different from the traditional studies that focus only on GNR material properties or two terminal devices. In addition, three typical defect locations in the channel, that is, 'near the source', 'mid-channel' and 'near the drain', are considered to examine the defect location influence. For all the defects, the atomic positions are relaxed, so that the calculations are performed based on their actual defect shapes instead of the ideal defect shapes.

2. Computational theory: The quantum-mechanics-based simulation consists of three steps. The first step is relaxation of the vacancy defects from their ideal defect shapes to their actual defect shapes. The second step is simulation of the effects of the vacancy defects on GNR material characteristics, such as band structure, which forms the base for studies of device characteristics. The last step is to analyse the defect effects on GNRFET device characteristics under the gate-source and drain-source voltages.

The density functional theory (which is based on the first principle) is adopted to accomplish the first two steps. According to the Hohenberg-Kohn theory [27], the ground state of a multi-body system can be described as the Hohenberg-Kohn energy functional

$$\begin{aligned} E[\rho, V] &= \langle \Psi[\rho] | T + V_{ee} + V_{ext} | \Psi[\rho] \rangle \\ &= T[\rho] + V_{ee}[\rho] + \int d^3 r V(\vec{r}) \rho(\vec{r}) \\ &= F[\rho] + \int d^3 r V(\vec{r}) \rho(\vec{r}) \end{aligned} \tag{1}$$

where ρ is the carrier density, $T[\rho]$ is the kinetic energy functional, $V_{ee}[\rho]$ is the potential energy functional and $F[\rho]$ is the functional composed of $T[\rho]$ and $V_{ee}[\rho]$. Equation (1) can be calculated through the Kohn-Sham equation [28].

To analyse the defect effects on GNRFET device characteristics (i.e. the third step), the non-equilibrium Green's function with tight binding Hamiltonian is utilised to study carrier transport under terminal voltages [29]. The Green's function of a device can be written as

$$G_d = \left(E - H_d - \Sigma_1 - \Sigma_2\right)^{-1} \tag{2}$$

© The Institution of Engineering and Technology 2013

doi: 10.1049/mnl.2013.0457

where E is the carrier energy, H_d is the device Hamiltonian and Σ_1 and Σ_2 are the self-energy terms. Once (2) is solved, the transmission coefficient can be obtained as

$$T = \text{Trace}\left(\Gamma_1 G_d \Gamma_2 G_d^{\dagger}\right) \tag{3}$$

where

$$\Gamma_{1,2} = i\left(\Sigma_{1,2} - \Sigma_{1,2}^{\dagger}\right)$$

is the broadening matrix of the terminals.

Finally, according to the Landauer-Büttiker formalism, the current under the terminal voltages can be calculated as

$$I = \frac{2e}{h}\int_{u_2}^{u_1} \mathrm{d}E\left[f_1(E,\ V) - f_2(E,\ V)\right]\cdot T \tag{4}$$

where u_1 and u_2 are the terminal chemical potentials, V is the bias voltage, $f_1(E, V)$ and $f_2(E, V)$ are the Fermi distributions on terminals, e is the electron charge and h is the Planck constant.

To realise the procedures described above, the Atomistic ToolKit was used as the platform to perform the numerical computations, in which the convergence criterion was set as 150Ry, the periodic boundary condition and generalised gradient approximation were used, and the exchange potential was dealt with by the Perdew-Burke-Ernzerhof method.

3. Effects on GNR

3.1. Vacancy defects in GNR: Defects can be classified as point defects, line defects and planar defects. Since the GNR is a quasi-one-dimensional nanometre material, point defects (e.g. vacancy defects, substitution defects and absorption defects) are the common ones. Here, four typical vacancy defects in GNR, including the SV defect, the DV defect, the SW defect and the 555 777 defect, are discussed. The substrate is assumed to be an armchair GNR (AGNR) structure since it is semiconducting and suitable for the device channel.

The SV defect is the simplest vacancy defect in GNR [11]. It is formed when one carbon atom is missed in the GNR. Owing to the interaction among the atoms around the defect (such as A and B in Fig. 1*a*), the shape of the SV defect will change [30]. The actual shape of the SV defect is determined through a relaxation procedure. After the relaxation, under the criterion of convergence (which is specified as the interaction among atoms being <0.02 eV/Å), the relaxed structure is as shown as Fig. 1*a*. As a result, the positions of the atoms around the defect are all re-adjusted, and bigger position changes occur for atoms closer to the defect. For example, atoms A and B deviate considerably from their initial lattice locations, whereas atom C almost stays at its original position. Specifically, the distance between A and B decreases from 2.461 to 1.809 Å.

If two carbon atoms are missed in a C–C chemical bond, a DV defect is formed. Again, because of the interaction among the surrounding atoms, the defect changes into a 5-8-5 structure, which is composed of two pentagons and an octagon [10, 11]. After the relaxation, the distance between A and B (or C and D) decreases from 2.461 to 1.632 Å as shown in Fig. 1*b*. When a C–C chemical bond is rotated 90°, a SW defect [31] is formed as in Fig. 1*c*. If a C–C chemical bond in the octagon of the DV defect is rotated as the SW defect, a 555 777 defect is formed, as shown in Fig. 1*d*. The C–C bond between A and B is rotated 90°, and three pentagons and three heptagons are formed after relaxation.

3.2. Effects on energy band structure: Since the energy band structure decides the basic electrical characteristics of the devices, the defect effects on the energy band are discussed in this Subsection. An AGNR with $N = 11$ (the carbon atom number in the width direction) and $L = 3$ (the unit cell number in the length direction) is used as the substrate.

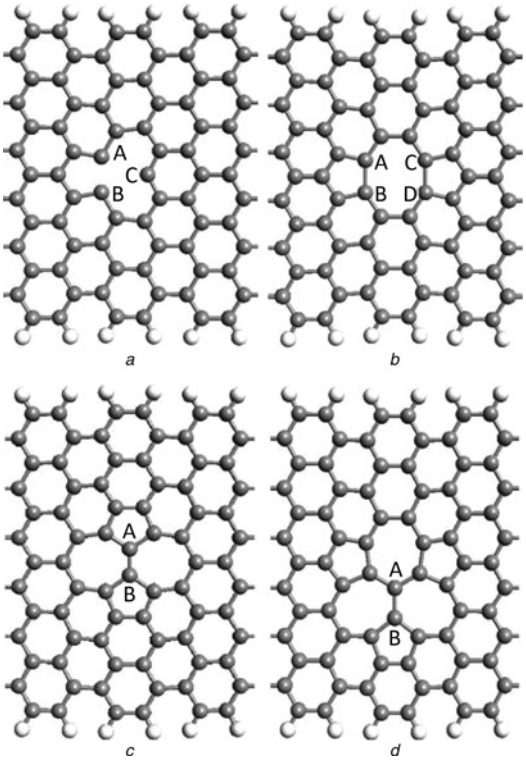


Figure 1 *Structure of the vacancy defects*
a SV defect
b DV defect
c SW defect
d 555 777 defect

To establish a reference, the energy band structure of the intact AGNR is plotted in Fig. 2*a*. The Fermi level is chosen as the reference energy level (i.e. energy level 0). The two lowest bands in the conduction band are labelled as α and β, and the two highest bands in the valence band are labelled as α' and β'. They are symmetrical with respect to the Fermi level, respectively. The bandgap is about 0.812 eV.

When the SV defect is introduced, the energy bands change greatly, as shown in Fig. 2*b*. At the K point (i.e. the point where $k = 0$), the Fermi level declines into the valence band, the α' band crosses the Fermi level and the β' band goes closer to the Fermi level. The influences on the α band and the β band are relatively minor, that is, only the energy levels are lifted. The calculated result shows that the bandgap is 0.189 eV narrower than the bandgap of the intact AGNR.

Fig. 2*c* shows the effects of the DV defect on the energy bands. In this case, the Fermi level is higher than the valence band, but the α' band intersects with the β' band. In addition, the DV defect has influence evident on the conduction band. The α band becomes almost a parallel line with the Fermi level. The bandgap is about 0.738 eV, which is also narrower than that in the intact AGNR.

Fig. 2*d* shows the effects of the SW defect on the energy bands. The Fermi level is approximately located at the middle between the valence band and the conduction band. The distance between the α band and the β band becomes larger, similar to the DV defect. The α' band and the β' band are degenerate at the K point. Different from the SV and the DV defects, the SW defect increases the bandgap by 0.031 eV.

The 555 777 defect has a significant influence on the valence band, as shown in Fig. 2*e*. The Fermi level passes through the valence band, and the α' band and the β' band are almost degenerate

© The Institution of Engineering and Technology 2013

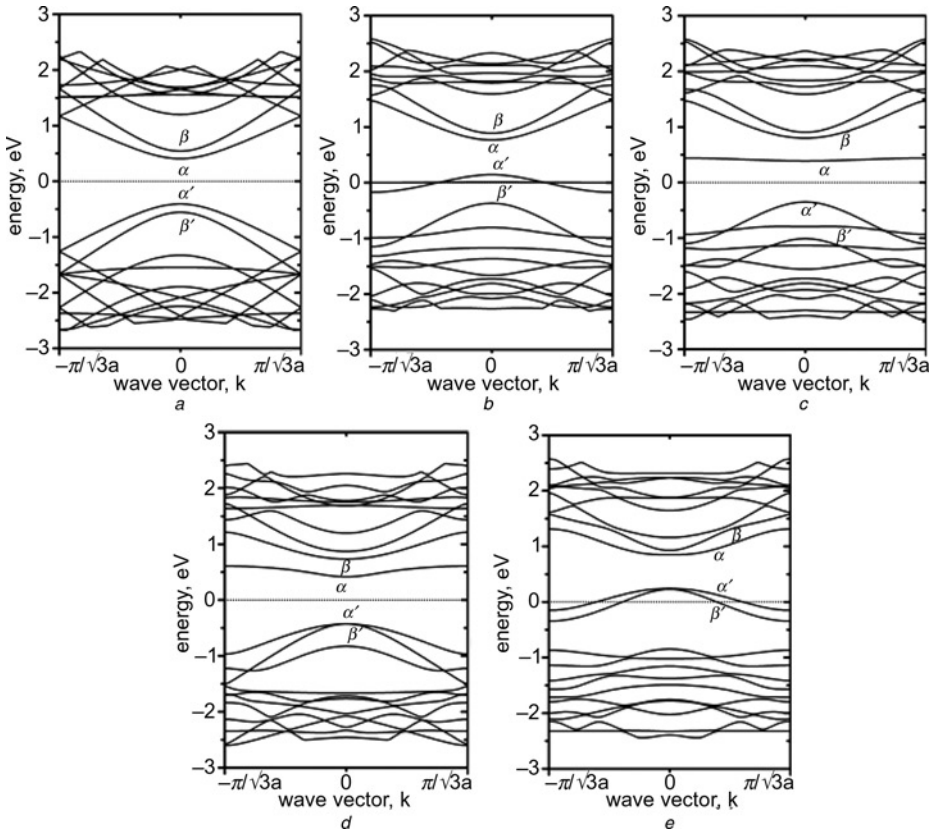


Figure 2 *Energy band structure of AGNR with N = 11 and L = 3*
a Intact AGNR
b SV defect AGNR
c DV defect AGNR
d SW defect AGNR
e 555 777 defect AGNR

at the K point. In addition, the 555 777 defect exhibits the most significant effect on the bandgap among all the four defects. The bandgap shrinks by about 0.205 eV.

From the above discussions, one can see that the 555 777 defect has the strongest effect on the energy bands, followed by the SV defect and the DV defect in the order of the impact's strength, whereas the SW defect has the weakest effect.

4. Effects on FET

4.1. Structure of the GNRFET: A 'Z' GNRFET [32] is used here to elucidate the defect effects. The channel is made of an armchair GNR, and the source and the drain are made of a zigzag GNR, which exhibits metallic characteristics regardless of its width. Since the sizes of modern silicon devices have achieved the nanometre scale, as a candidate for future nanoscale devices, the size of the GNRFET is assumed to be small. The structure of the GNRFET is shown as Fig. 3 and its parameters are listed in Table 1.

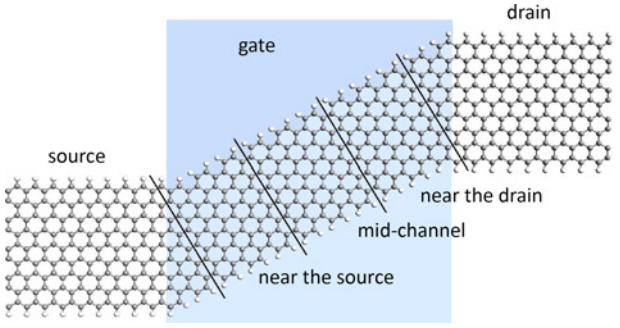


Figure 3 *Three defect locations in the GNRFET channel*

To study the defect effects in depth, three different locations of the defects in the channel are assumed. As shown in Fig. 3, these three locations are 'near the source', 'mid-channel' and 'near the drain'. In the three parts of the channel, the part with the defects is relaxed as discussed in the preceding Section, whereas the other two parts remain intact.

4.2. Effects on transmission coefficient: According to the Landauer-Büttiker formula, the channel current is tightly related to the transmission coefficient. Hence, the effects of the defects on the transmission coefficient are analysed in this Subsection.

Different from the traditional FETs, the GNRFET exhibits bipolar characteristics, implying that the electron is the major carrier under the high gate-source voltage and the hole is the major carrier under the low gate-source voltage. Without loss of generality, Vgs is set as 0.2 V to be a typical low-voltage condition for the hole current and 0.9 V to be a typical high-voltage condition for the electron current, whereas Vds is set as 0.6 V for all the calculations in this Subsection.

Fig. 4 plots the transmission coefficients under the SV defects at various locations, that is, 'near the source', 'mid-channel' and 'near

Table 1 Parameters of the GNRFET

Channel	Material	13-AGNR
Gate	Width	4.53 nm
	Length	3.94 nm
Insulator	Material	$HfO_2(k = 16)$
	Thickness	1 nm
Source/drain	Material	9-ZGNR

© The Institution of Engineering and Technology 2013

doi: 10.1049/mnl.2013.0457

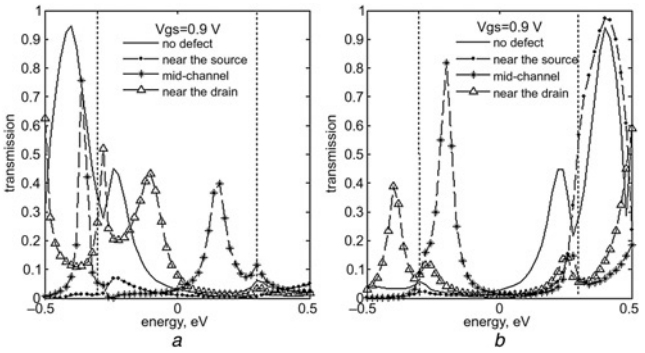


Figure 4 *Transmission coefficients under the SV defects at various locations*
a Hole as major carrier
b Electron as major carrier

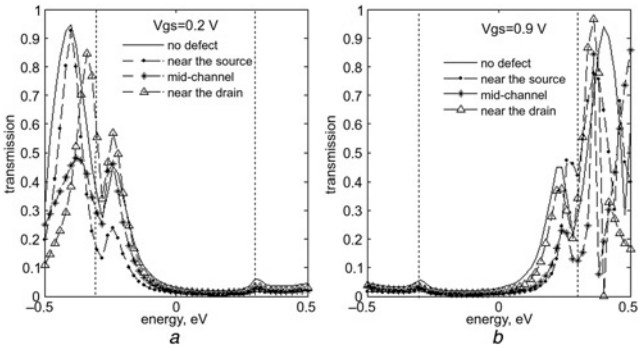


Figure 6 *Transmission coefficients under the SW defects at various locations*
a Hole as major carrier
b Electron as major carrier

the drain' in the channel. The transmission coefficient of the intact GNRFET without any defect is shown as a reference. The Fermi level is chosen as the reference energy level (i.e. energy level 0). Two vertical dotted lines are drawn as indications of chemical potentials of source and drain. Only the transmissions between these two lines have contributions to the channel current according to the Landauer-Büttiker formula. Hence, only the transmissions in this interval need to be considered.

From Fig. 4, one can observe that a significant peak in the transmission coefficient appears when the SV defect is halfway through the channel, regardless of whether the hole or the electron is the major carrier. In light of the discussion in the preceding Section, it is because the Fermi level declines into the valence band and thus a bigger channel current is produced. When the SV defect is near the source, the hole transmission is obviously restrained. When the SV defect is near the drain, on the other hand, the electron transmission is restrained evidently. Since the hole has the reverse motion direction with the electron, it can be concluded that the SV defect restrains the carrier's transmission when it is located near the end of a transmission.

Fig. 5 depicts the transmission coefficients under the DV defects at various locations in the channel. Since the Fermi level is in the bandgap, no peak apparently occurs in the transmission. In fact, the transmission coefficients under the DV defect at various locations are much smaller than those in the intact GNRFET, particularly for the hole as the major carrier. That is, the DV defect can decrease the channel current.

Fig. 6 plots the transmission coefficients under the SW defects at various locations in the channel. No significant difference can be observed by comparison with the intact GNRFET, although the overall transmission coefficients decrease slightly. This is consistent with the conclusion that the SW defect has the weakest effect as discussed in the preceding Section on the energy band structure.

Fig. 7 shows the transmission coefficients under the 555 777 defects at various locations in the channel. Similar to the SV defect, a big peak occurs when the 555 777 defect is halfway through the channel. Again, it is because the Fermi level declines into the valence band and thus the channel current increases considerably. For the other defect locations, however, the effects of the 555 777 defect are nothing similar to those of the SV defect. When the 555 777 defect is near the source, the hole transmission is restrained, but it is weaker than that of the SV defect. When it is near the drain, the transmission coefficient is even bigger than that in the intact GNRFET. An explanation about this phenomenon is that because the size of the 555 777 defect is so big, it almost touches the source or drain area when it is near the terminals of the channel. Noting that the source or drain area is a region of ZGNR, the defect is influenced by the ZGNR.

4.3. Effects on transfer characteristics: Transfer characteristics are one of the most primary parameters for FETs. The effects of the defects at various locations on the transfer characteristics are analysed under different drain-source voltages in this Subsection.

Fig. 8 depicts the transfer characteristics of the GNRFET with the SV defects at various locations in the channel under different *V*ds. When the defect is halfway through the channel, its effect on the transfer characteristics is subversive, as shown in Fig. 8*a*. For all drain-source voltages, the channel current significantly increases near the Dirac point, and destroys the 'V' shape of the bipolar characteristics, which can be attributed to the elevated peak of the transmission coefficient as shown in Fig. 4.

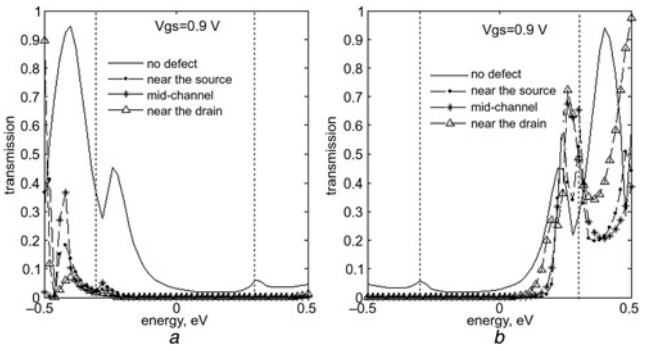


Figure 5 *Transmission coefficients under the DV defects at various locations*
a Hole as major carrier
b Electron as major carrier

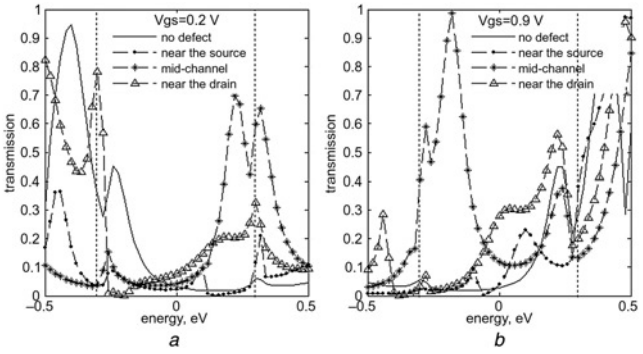


Figure 7 *Transmission coefficients under the 555 777 defects at various locations*
a Hole as major carrier
b Electron as major carrier

© The Institution of Engineering and Technology 2013

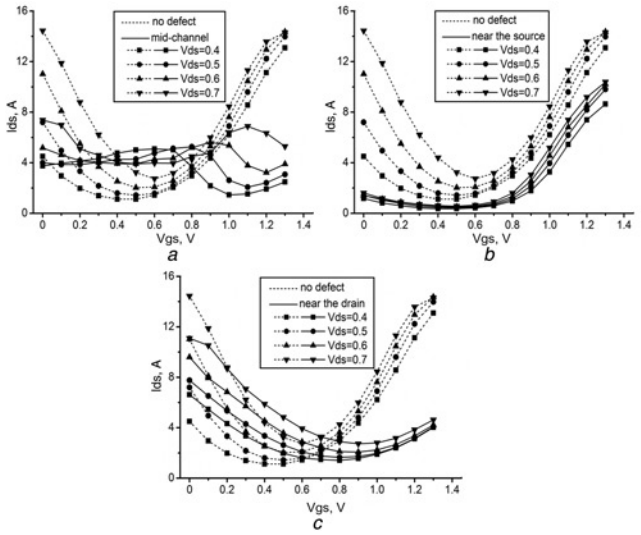


Figure 8 *Transfer characteristics for the SV defects at various locations*
a In the mid-channel
b Near the source
c Near the drain

As shown in Fig. 8*b*, when the SV defect is near the source, the channel current decreases for all the drain-source voltages. Moreover, the reduction of the hole current (i.e. on the left side of the Dirac point) exceeds the reduction of the electron current (i.e. on the right side of the Dirac point), which agrees with the analysis of the transmission coefficient in the preceding Subsection.

Fig. 8*c* plots the transfer characteristics of the GNRFET when the SV defect is near the drain under different Vds. In this case, the electron current is restrained. The hole current increases for some Vgs (e.g. 0.3 V < Vgs < 0.7 V when Vds = 0.7 V), which can be justified by the analysis of the transmission coefficient (i.e. there are two peaks in Fig. 4*a*).

Another interesting result is the drift of the Dirac point to a higher voltage by comparison with the intact GNRFET. Note that the Dirac point is a bias voltage condition where the hole current is equal to the electron current. When the SV defect presents, the

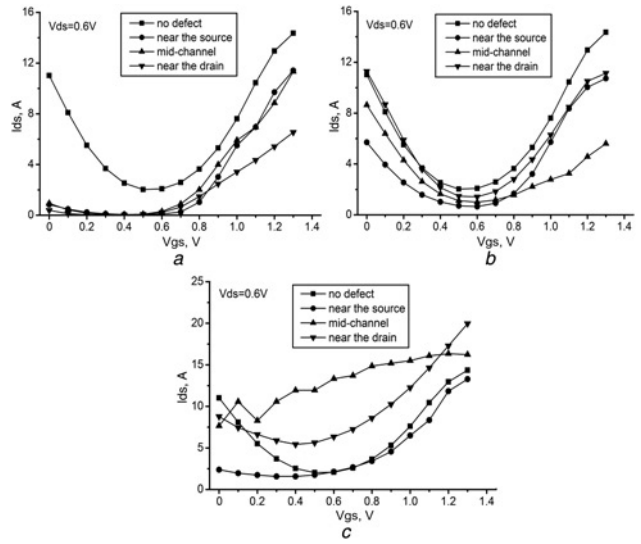


Figure 9 *Transfer characteristics for different defects at various locations*
a DV defects
b SW defects
c 555 777 defects

Table 2 Major effects on the transfer characteristics

	Near the source	Mid-channel	Near the drain
SV defect	restrain hole current	destroy 'V' shape	drift Dirac point
DV defect	restrain hole current	restrain hole current	restrain hole current
SW defect	reduce total current	reduce total current	reduce total current
555 777 defect	restrain hole current	destroy 'V' shape	increase total current

Fermi level descends into the valence band and the transmission region moves towards the high energy terminal. To achieve the Dirac point, some mechanism is needed to balance the hole and the electron currents. When the SV defect is near the source, the mechanism is fulfilled by the defect's restraint on the hole current, and thus the Dirac point is relatively stable. When the SV defect is near the drain, the electron current is restrained. Increasing the gate-source voltage to boost the electron current is the way to balance the hole and the electron currents, and thus the Dirac point drift to a higher voltage.

As shown in Fig. 8, the transfer characteristics under different drain-source voltages result in similar curves. Without loss of generality, the drain-source voltage is hereinafter fixed at 0.6 V in the following analysis for the other three types of vacancy defects.

Fig. 9*a* compares the transfer characteristics of the GNRFET for the DV defects at various locations in the channel with those of the intact GNRFET. From it, one can observe that the minimum current is remarkably decreased because of the fact that the hole and the electron currents are restrained severely. This can be explained by the suppressed transmission coefficients, as shown in Fig. 5, for the DV defect.

Fig. 9*b* compares the transfer characteristics of the GNRFET for the SW defects at various locations in the channel with those of the intact GNRFET. Similar to the preceding discussions on the energy band and the transmission coefficient, the SW defect has a very minor effect on the transfer characteristics. The channel current decreases evidently only when Vgs is high.

Fig. 9*c* plots the transfer characteristics of the GNRFET for the 555 777 defects at various locations in the channel by comparison with those of the intact GNRFET. Similar to the SV defect, the 'V' shape of the bipolar characteristics is destroyed when the 555 777 defect is located halfway through the channel since the Fermi level descends into the valence band. When the 555 777 defect is near the drain, the channel current becomes larger than that in the intact GNRFET, whereas the 'V' shape of the transfer characteristics is maintained. When the 555 777 defect is near the source, the hole current is restrained.

Based on the discussions above, generally speaking, each type of defect influences the transfer characteristics of the GNRFET in multiple ways, such as reducing the total current, drifting the Dirac point and so on. The major effects of these defects on the transfer characteristics are summarised in Table 2.

5. Conclusion: As the most common vacancy defects in graphene, the SV defect, the DV defect, the SW defect and the 555 777 defect have been examined and, in particular, their effects on GNR and GNRFET have been studied in detail. The energy band structure, the transmission coefficient and the transfer characteristics can all be changed by these defects. Among them, the 555 777 defect has the strongest effect, whereas the SW defect has the weakest effect. When the defects are halfway through the channel, severer effects can be observed by comparison with those when the defects are near the source or the drain in the channel. This study has revealed the important effects of the vacancy defects in the

© The Institution of Engineering and Technology 2013

doi: 10.1049/mnl.2013.0457

GNRFET, and can provide guidelines for designs and the fabrication of graphene-based devices.

6. Acknowledgments: This work was supported by the National Natural Science Foundation of China (grant nos 61204096 and 61331007) and the Specialised Research Fund for the Doctoral Program of Higher Education (grant nos 20100141120040 and 20110141120074).

7 References

[1] Novoselov K.S., Geim A.K., Morozov S.V., *ET AL.*: 'Electric field effect in atomically thin carbon films', *Science*, 2004, **306**, pp. 666–669

[2] Meric I., Dean C.R., Han S.J., *ET AL.*: 'High-frequency performance of graphene field effect transistors with saturating IV-characteristics'. IEEE Int. Electron Devices Meeting (IEDM), Washington DC, USA, 2011, pp. 2.1.1–2.1.4

[3] Lemme M.C., Echterneyer T.J., Baus M., Kurz H.: 'A graphene field-effect device', *IEEE Electron Device Lett.*, 2007, **28**, pp. 282–284

[4] Kim S., Nah J., Jo I., *ET AL.*: 'Realization of a high mobility dual-gated graphene field-effect transistor with Al_2O_3 dielectric', *Appl. Phys. Lett.*, 2009, **94**, p. 062107–3

[5] Han M.Y., Özyilmaz B., Zhang Y., Kim P.: 'Energy band-gap engineering of graphene nanoribbons', *Phys. Rev. Lett.*, 2007, **98**, p. 206805

[6] Li X., Wang X., Zhang L., Lee S., Dai H.: 'Chemically derived, ultrasmooth graphene nanoribbon semiconductors', *Science*, 2008, **319**, pp. 1229–1232

[7] Wang X., Ouyang Y., Li X., Wang H., Guo J., Dai H.: 'Room temperature all-semiconducting sub 10 nm graphene nanoribbon field effect transistors', *Phys. Rev. Lett.*, 2008, **100**, p. 206803

[8] Ryzhii V., Ryzhii M., Satou A., Otsuji T.: 'Current-voltage characteristics of a graphene-nanoribbon field-effect transistor', *J. Appl. Phys.*, 2008, **103**, p. 094510

[9] Fiori G.: 'Simulation of graphene nanoribbon field-effect transistors', *IEEE Electron Device Lett.*, 2007, **28**, pp. 760–763

[10] Kim Y., Ihm J., Yoon E., Lee G.D.: 'Dynamics and stability of divacancy defects in graphene', *Phys. Rev. B*, 2011, **84**, p. 075445

[11] Kotakoski J., Krasheninnikov A.V., Kaiser U., Meyer J.C.: 'From point defects in graphene to two-dimensional amorphous carbon', *Phys. Rev. Lett.*, 2011, **106**, p. 105505

[12] Hashimoto A., Suenaga K., Gloter A., Urita K., Iijima S.: 'Direct evidence for atomic defects in graphene layers', *Nature*, 2004, **430**, pp. 870–873

[13] Brenner K., Murali R.: 'In situ doping of graphene by exfoliation in a nitrogen ambient', *Appl. Phys. Lett.*, 2011, **98**, p. 113115

[14] Zhang C., Fu L., Liu N., Liu M., Wang Y., Liu Z.: 'Synthesis of nitrogen-doped graphene using embedded carbon and nitrogen sources', *Adv. Mater.*, 2011, **23**, pp. 1020–1024

[15] Li L., Reich S., Robertson J.: 'Defect energies of graphite: density functional calculations', *Phys. Rev. B*, 2005, **72**, p. 184109

[16] Ataca C., Akturk E., Şahin H., Ciraci S.: 'Adsorption of carbon adatoms to graphene and its nanoribbons', *J. Appl. Phys.*, 2011, **109**, p. 013704

[17] Rutter G.M., Crain J.N., Guisinger N.P., Li T., First P.N., Stroscio J. A.: 'Scattering and interference in epitaxial graphene', *Science*, 2007, **317**, pp. 219–222

[18] Pereira V.M., Guinea F., Lopes Dos Santos J.M.B., Peres N.M.R., Castro Neto A.H.: 'Disorder induced localized states in graphene', *Phys. Rev. Lett.*, 2006, **96**, p. 036801

[19] Magna A.L., Deretzis I., Forte G., Pucci R.: 'Conductance distribution in doped and defected graphene nanoribbons', *Phys. Rev. B*, 2009, **80**, p. 195413

[20] Ihnatsenka S., Kirczenow G.: 'Conductance quantization in strongly disordered graphene ribbons', *Phys. Rev. B*, 2009, **80**, p. 201407(R)

[21] Gorjizadeh N., Farajian A.A., Kawazoe Y.: 'The effects of defects on the conductance of graphene nanoribbons', *Nanotechnology*, 2009, **20**, p. 015201

[22] Deretzis I., Fionri G., Iannaccone G., La Magna A.: 'Effects due to backscattering and pseudogap features in graphene nanoribbons with single vacancies', *Phys. Rev. B*, 2010, **81**, p. 085427

[23] Bahamon D.A., Pereira A.L.C., Schulz P.A.: 'Tunable resonances due to vacancies in graphene nanoribbons', *Phys. Rev. B*, 2010, **82**, p. 165438

[24] Ma K.L., Yan X.H., Xiao Y., Chen Y.P.: 'Electronic transport properties of metallic graphene nanoribbons with two vacancies', *Solid State Commun.*, 2010, **150**, pp. 1308–1312

[25] Ren Y., Chen K.Q.: 'Effects of symmetry and Stone-Wales defect on spin-dependent electronic transport in zigzag graphene nanoribbons', *J. Appl. Phys.*, 2010, **107**, p. 044514

[26] Yoon Y., Fiori G., Hong S., Iannaccone G., Guo J.: 'Performance comparison of graphene nanoribbon FETs with Schottky contacts and doped reservoirs', *IEEE Trans. Electron Devices*, 2008, **55**, pp. 2314–2323

[27] Hohenberg P., Kohn W.: 'Inhomogeneous electron gas', *Phys. Rev.*, 1964, **136**, pp. B864–B871

[28] Kohn W., Sham L.J.: 'Self-consistent equations including exchange and correlation effects', *Phys. Rev.*, 1965, **140**, pp. A1133–A1138

[29] Wang H., Wang G., Chang S., Huang Q.: 'High-order element effects of the Green's function in quantum transport simulation of nanoscale devices', *IEEE Trans. Electron Devices*, 2009, **56**, pp. 3106–3114

[30] Meyer J.C., Kisielowski C., Erni R., Rossell M.D., Crommie M.F., Zettl A.: 'Direct imaging of lattice atoms and topological defects in graphene membranes', *Nano Lett.*, 2008, **8**, pp. 3582–3586

[31] Stone A.J., Wales D.J.: 'Theoretical studies of icosahedral C60 and some related species', *Chem. Phys. Lett.*, 1986, **128**, pp. 501–503

[32] Yan Q., Huang B., Yu J., *ET AL.*: 'Intrinsic current – voltage characteristics of graphene nanoribbon transistors and effect of edge doping', *Nano Lett.*, 2007, **7**, pp. 1469–1473

© The Institution of Engineering and Technology 2013